International Journal of Thermal Sciences 110 (2016) 369–382

Contents lists available at ScienceDirect

International Journal of Thermal Sciences

journal homepage: www.elsevier.com/locate/ijts

Flow control through the use of heterogeneous porous media: “Smart” passive thermo-insulating materials

Yosef Gulberg, Yuri Feldman*

Department of Mechanical Engineering, Ben-Gurion University of the Negev, P.O. Box 653, Beer-Sheva, 84105, Israel

ARTICLE INFO

Article history:
Received 8 February 2016
Received in revised form
6 July 2016
Accepted 18 July 2016
Available online 3 August 2016

Keywords:
Passive flow control
Heterogeneous porous media
Linear stability analysis
“Smart” thermal insulators

ABSTRACT

In this paper, the concept of “smart” thermally insulating materials intelligently adapted to specific engineering configurations is established and extensively validated. Thermal insulation is achieved by local suppression of the momentum of the confined natural convection flow in the most critical regions, as determined by a linear stability analysis of the flow in the presence of implants of heterogeneous porous media. The implants are modelled by unconnected packed beds of equi-sized cylinders. The concept is based on a mesoscale approach in which the non-slip boundary conditions in the vicinity of the packed beds are explicitly imposed by utilizing the immersed boundary (IB) method. Two different patterns for the “smart” porous media are established, and their thermal insulation properties are quantified. It is shown that the optimized patterns for implants of heterogeneous porous media, occupying approximately only 5% of the overall volume, can drastically delay the steady-unsteady transition of the 2*D* natural convection flow in a square differentially heated cavity with thermally perfectly conducting horizontal walls. In addition, it is demonstrated that the implants facilitate a consistent decrease in the heat flux through a cubic differentially heated cavity with all being thermally perfectly conducting lateral walls.

1. Introduction

Utilizing porous media for the enhancement of flow control in a wide spectrum of scientific and engineering fields has gained a considerable attention in the past two decades. We cite, for example, studies aimed to: control heat flux rates in confined [1,2] and open [3] natural convection flows; investigate means for wake regularization and reducing the drag coefficient of incident flows around bluff bodies [4]; control the velocity profile in industrial crossflow filtration systems [5]; delay the transition to turbulence over the surface of a wing [6]; determine the axial pressure distribution of fluid transport in blood vessels [7]; and characterize the flow and transport through fractured geological formations [8].

Traditionally, the analysis of flow and heat transfer in porous media is based on applying volume-averaging techniques to fluid flow equations. In such cases, the complex geometry of solid boundaries is modelled by assuming a continuous phase that overlaps solid and fluid regions and is treated by macroscopic averaged equations (see e.g., [9–14]). Flow fields near the solid boundaries are not resolved explicitly, and interface effects are modelled by a priori provided correlations. The drawback of volume-averaging techniques is their lack of generality, resulting from the considerable morphological variations of porous materials. Therefore, important flow characteristics of a particular porous material can be predicted accurately only if the corresponding experimental data is available. However, experimental data is typically acquired for specific porous materials and flow conditions, thereby severely restricting the application of volume-averaging techniques.

A mesoscale approach, explicitly resolving the flow near solid surfaces, offers an alternative to the volume-averaging technique. This approach has gained popularity in the past decade with the rapid development of computational power. Studies performed to date typically treat porous materials as composite voids and beds of solid particles and address the flow through ordered, staggered or randomly packed beds of different particle shapes that correspond to various porous media configurations. Although the mesoscale modeling of porous media is typically restricted to non-contacting packed beds of solid particles, the characteristic distance between the particles is sufficiently close to significantly affect the heat and

* Corresponding author.
E-mail address: yurifeld@bgu.ac.il (Y. Feldman).

http://dx.doi.org/10.1016/j.ijthermalsci.2016.07.008
1290-0729/

mass transfer processes. This allows for further generalization of the obtained results to elucidate the fundamental macroscale mechanisms and geometrical characteristics of the corresponding heterogeneous porous media. Results obtained by mesoscale analysis are widely utilized for developing universal macro correlations for estimating the following: the average Nusselt number of the natural convection process inside porous enclosures [15], the pressure gradient for a wide range of Reynolds numbers [16–18], the flow dispersivity [19], the drag force exerted by the flow on the porous medium [20–22], and finally the permeability of various porous media configurations [20,23–27]. Another widely used application of the mesoscale approach is related to the passive control of confined natural convection flows in terms enhancement of their thermo-insulating efficiency. Research in this area is motivated mainly by the need to control the heat flux through confined enclosures partially filled with solid products of various forms, orientations and distributions and is relevant to indoor environmental control [28,29], refrigeration equipment and thermal management of greenhouses [30], cooling of electronic devices [31,32], etc.

The present paper reports our efforts to develop a systematic methodology based on a mesoscale approach to control incompressible natural convection flows in confined enclosures by exploiting heterogeneous porous media. This task has so far been performed only heuristically, attributing the reduced heat flux to the blocking effects of solid non-connected obstacles and the redirection of the flow away from the vertical cold and hot walls toward the cavity center. The principal novelty of the present study lies in the control of the flow by intelligent suppression of the fluctuations of the major flow characteristics (for example, perturbations of velocity components, temperature, pressure, or their combinations) in the most critical regions, as determined by linear stability analysis. Intelligent control is facilitated by explicit placing of the heterogeneous porous media, whose geometry characteristics have been optimized for the specific flow configuration, into the bulk natural convection flow. Porous media implants, created by this methodology, form the basis of the concept of "smart" thermo-insulating materials, which intelligently suppress the oscillations of the thermal flow in accordance with given optimization criteria. The efficiency of the proposed concept of "smart" thermo-insulation is demonstrated by applying it to the natural convection flow in square (for $2D$) and cubic (for $3D$) differentially heated cavities. It is shown that optimized non-homogenous porous media implants, occupying approximately only five percent of the overall volume, can drastically delay the steady-unsteady transition of the $2D$ natural convection flow and produce a consistent decrease of the heat flux through a cubic differentially heated cavity with all being thermally perfectly conducting lateral walls.

2. Theoretical background

The methodology for the intelligent control of heat flux in confined natural convection flows, developed in the framework of the present study, is based on a linear stability analysis of natural convection flows in the presence of heterogeneous porous media. The heterogeneous porous media are modelled by implants consisting of unconnected packed beds of circular equi-sized cylinders. The heterogeneous spatial distribution of the cylinders inside the implants is a function the two optimisation criteria, as follows. The first criterion, **A**, is defined as $\mathbf{A} = \left|u_x{'}\right|^2 + \left|u_y{'}\right|^2$, where $|u_x{'}|$ and $\left|u_y{'}\right|$ are the absolute values of the perturbations of the corresponding velocity components. The idea originates from the definition of the turbulent kinetic energy, $e_k{'}$, which is equal to the sum of the squares of the fluctuations of the velocity components, although the proposed criterion, **A**, cannot be formally related to $e_k{'}$ due to the phase differences between $|u_x{'}|$ and $\left|u_y{'}\right|$. The second criterion, **B**, is directly related to the absolute value of the perturbation of the temperature field $\mathbf{B} = |\theta'|$. The insulating efficiency of the embedded porous implants, whose patterns are designed in accordance with the two criteria, is discussed in the following sections.

2.1. Governing equations

The mesoscale approach utilized in the present study for the simulation of the natural convection flow in porous media requires that we explicitly impose the no-slip constraint on all the surfaces of the unconnected packed beds. The requirement is satisfied by utilizing the immersed boundary (IB) method introduced by Peskin [33]. No-slip boundary conditions are set at all external walls of the computational domain. In accordance with the formalism of the IB method, the unconnected packed beds immersed in the convective flow are determined by a set of Lagrangian boundary points that do not necessarily coincide with the underlying Eulerian grid. This requires the introduction of additional terms and relationships, corresponding to interpolation and regularization operators, to convey information to and from the immersed surfaces. Applying the Boussinesq approximation for simulation of the buoyancy effects, the unsteady natural convection flow with the embedded IB functionality is governed by the following system of continuity, Navier-Stokes (NS), and energy equations (Eqs. (1)–(3)), and by Eqs. (4) and (5), which are introduced to satisfy the kinematic constraints of no-slip and the determined temperature (or heat flux) boundary conditions on the surfaces of the embedded unconnected packed beds that model implants of porous media:

$$\nabla \cdot \boldsymbol{u} = 0 \tag{1}$$

$$\frac{\partial \boldsymbol{u}}{\partial t} + (\boldsymbol{u} \cdot \nabla)\boldsymbol{u} = -\nabla p + \sqrt{\frac{Pr}{Ra}}\nabla^2 \boldsymbol{u} + \theta \vec{e}_y + \boldsymbol{f} \tag{2}$$

$$\frac{\partial \theta}{\partial t} + (\boldsymbol{u} \cdot \nabla)\theta = \frac{1}{\sqrt{PrRa}}\nabla^2 \theta + q \tag{3}$$

$$\boldsymbol{U}_b(\boldsymbol{X}_k) = \boldsymbol{I}(\boldsymbol{u}(\boldsymbol{x})) \tag{4}$$

$$\Theta_b(\boldsymbol{X}_k) = \boldsymbol{I}(\theta(\boldsymbol{x})), \tag{5}$$

where $\boldsymbol{u}=(u,v,w)$, p, t, and θ are the non-dimensional velocity, pressure, time and temperature, respectively, and $\vec{e}_y$ is a unit vector in the vertical (y) direction. The temperature-density coupling is implemented by applying the Boussinesq approximation $\rho = \rho_0(1\text{-}\beta(T-T_c))$. The problem is scaled by L, $U = \sqrt{g\beta L\Delta T}$, $t = L/U$, and $P = \rho U^2$ for length, velocity, time, and pressure,[1] respectively. Here, L is the length of the square differentially heated cavity (which is further used as test bed in our numerical experiments), ρ is the mass density of the wotking fluid, g is the gravitational acceleration, β is the isobaric coefficient of thermal expansion, and $\Delta T = T_h - T_c$ is the temperature difference between the hottest and coldest boundaries. The non-dimensional temperature θ is defined as $\theta = (T-T_c)/\Delta T$. The Rayleigh, Ra, and Prandtl, Pr, numbers are $Ra = \frac{g\beta}{\nu\alpha}\Delta T L^3$ and $Pr=\nu/\alpha$, respectively, where ν is the

[1] Note that the normalized pressure field contains both hydrostatic and hydrodynamic components.

kinematic viscosity and α is the thermal diffusivity. All the simulations were performed for $Pr = 0.71$, corresponding to air. The force $\boldsymbol{f}$ and the heat source q, appearing as volumetric sources in Eqs. (2) and (3), reflect the impact of the immersed surfaces of the porous media on the surrounding flow. These sources are not known a priori and are an inherent part of the overall solution, along with the unknown velocity, temperature and pressure fields. Equations (4) and (5) provide additional relationships between the Eulerian velocity $\boldsymbol{u}(\boldsymbol{x})$ and the temperature $\theta(\boldsymbol{x})$ fields interpolated on the Lagrangian points $\boldsymbol{X}^k$ to achieve closure of the overall system.

In practice, both interpolation and regularization of the desired quantity are implemented by calculation of the corresponding volume integrals involving convolution of the quantity with the discrete function δ. These integrals determine the interpolation $\boldsymbol{I}$ and regularization $\boldsymbol{R}$ operators as:

$$\boldsymbol{I}(\boldsymbol{u}(\boldsymbol{x}_i), \theta(\boldsymbol{x}_i)) = \int_{\Omega} (\boldsymbol{u}(\boldsymbol{x}), \theta(\boldsymbol{x})) \cdot \delta\left(\boldsymbol{X}^k - \boldsymbol{x}_i\right) dV_{\Omega i} = (\boldsymbol{U}_b, \Theta_b), \tag{6a}$$

$$\boldsymbol{R}\left(\boldsymbol{F}^k\left(\boldsymbol{X}^k\right), Q^k\left(\boldsymbol{X}^k\right)\right) = \int_{S} \left(\boldsymbol{F}^k\left(\boldsymbol{X}^k\right), Q^k\left(\boldsymbol{X}^k\right)\right) \cdot \delta\left(\boldsymbol{x}_i - \boldsymbol{X}^k\right) dV_S^k = (\boldsymbol{f}, q), \tag{6b}$$

where Ω and S correspond to the Eulerian and Lagrangian cells, respectively, $dV_{\Omega i}$ is the volume of the corresponding Eulerian cell, and dV_S^k corresponds to the virtual volume surrounding each Lagrangian point k (see Fig. 1 for additional details). The interpolation operator $\boldsymbol{I}$ in Eqs. (4) and (5) is used to satisfy the prescribed values of the surface velocity $\boldsymbol{U}_b$ and the surface temperature Θ_b. The regularization operator $\boldsymbol{R}$ is used in the calculation of the volumetric force $\boldsymbol{f}$ and the volumetric heat source q in Eqs. (2) and (3). The type of interaction between the immersed surface and the surrounding flow is determined by the specific choice of the delta function. In the present study, we used the discrete delta function introduced by Roma et al. [34].

$$d(r) = \begin{cases} \dfrac{1}{6\Delta r}\left[5 - 3\dfrac{|r|}{\Delta r} - \sqrt{-3\left(1 - \dfrac{|r|}{\Delta r}\right)^2 + 1}\right] & \text{for } 0.5\Delta r \le |r| \le 1.5\Delta r, \\ \dfrac{1}{3\Delta r}\left[1 + \sqrt{-3\left(\dfrac{r}{\Delta r}\right)^2 + 1}\right] & \text{for } |r| \le 0.5\Delta r, \\ 0 & \text{otherwise}, \end{cases} \tag{7}$$

where Δr is the cell width in the r direction. The accuracy of the chosen delta function has been successfully verified in a number of previous studies [35–39]. This delta function was specifically derived for use on staggered grids and involves only three cells in each computational direction, which significantly boosts its computational efficiency. We note in passing that to achieve high accuracy, the method should be implemented on a uniform grid in the vicinity of the immersed body surface, which is an intrinsic limitation of the delta function utilized. As a result, the Δl value corresponding to the distance between neighboring points of the immersed surface and the size of the Eulerian grid cell adjacent to the immersed surface should be approximately the same (i.e., $\Delta l \approx \Delta x = \Delta y = \Delta z$ and $dV_S^k \approx dV_{\Omega i}$, see Fig. 1 for additional details). Away from the body, non-uniform spatial discretization can be utilized. In the present study, we used the same delta functions for interpolation and regularization operators as those proposed by Peskin [33] and Beyer and LeVeque [40].

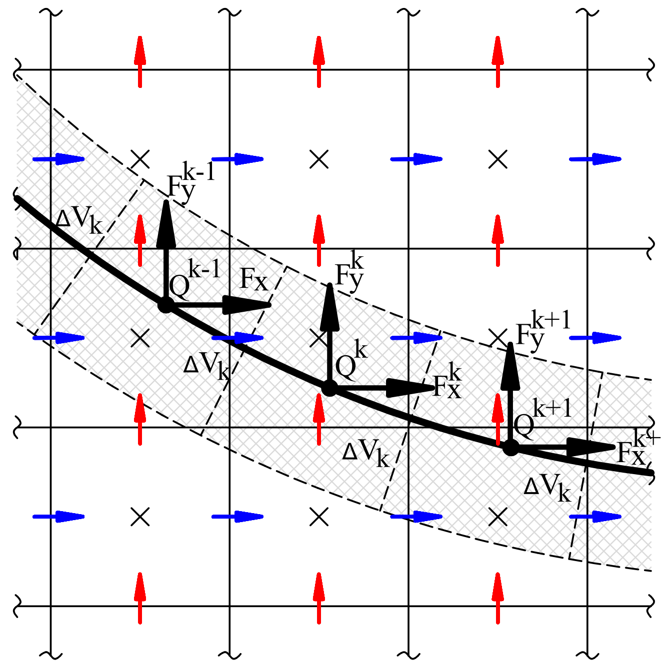

Fig. 1. Schematic representation of a staggered grid discretization of a two-dimensional computational domain D with a segment of an immersed boundary of a body B. A virtual shell, whose thickness is equal to the grid cell width, is shaded. The horizontal blue and vertical red arrows ($\rightarrow, \uparrow$) represent the discrete u_i and v_i velocity locations, respectively. Pressure p_i and temperature T_i are applied at the center of each cell ($\times$). Lagrangian points $\boldsymbol{X}^k(X^k, Y^k)$ along ∂B are shown as black circles • where the volumetric boundary forces $\boldsymbol{F}^k = (F_x^k, F_y^k)$ ($\rightarrow, \uparrow$) and the volumetric boundary heat sources Q^k are applied. (For interpretation of the references to colour in this figure legend, the reader is referred to the web version of this article.)

2.2. Numerical solution

Embedding the IB functionality into NS equations (1)–(5) can be implemented either implicitly, based on the Lagrange multiplier approach [39,41,42], or explicitly utilizing the direct forcing approach [43,44]. The present study used both formulations to establish and formally validate the concept of "smart" thermal insulators. The key idea is to locally suppress the most energetic regions of the convective flow, formally revealed by the linear stability analysis of the two-dimensional convective flow in the presence of immersed bodies of arbitrary shapes. The bodies play the role of local unconnected obstacles, suppressing the momentum of the convective flow. The linear stability analysis was performed by applying a linear stability solver with the embedded IB functionality recently developed by Feldman and Gulberg [39]. The solver is based on fully implicit coupling of the pressure and velocity fields. Kinematic constraints of no-slip and temperature boundary conditions are satisfied by introducing additional unknowns in the form of Lagrange multipliers. Although the solver was extensively verified for both isothermal and natural convection flows in our previous work [39], a verification study for the configuration relevant to the present research was performed for the sake of completeness, as detailed in the next section.

The assumption underlying the basis of the present study is that the linear stability analysis predicting the most energetic regions for the two-dimensional confined natural convection flow will also be valid for the three-dimensional configurations built by extension of the corresponding two-dimensional confinement along its normal direction. The idea originates from the striking

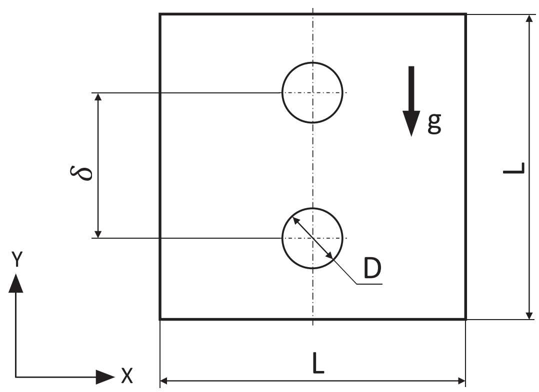

Fig. 2. Schematic representation of a geometrical model of the computational domain showing vertically aligned cylinders confined in a square cavity. Arrow indicates the direction in which the force of gravity acts.

similarity between the spatial and temporal characteristics observed for two- and three-dimensional steady and bifurcated flows in differentially heated square and cubic cavities, respectively, with perfectly thermally conducting horizontal boundaries, see e.g. Ref. [45]. The assumption made in the present study was validated by simulation of three-dimensional natural convection flows in a differentially heated cubic cavity with embedded cylindrical obstacles, the location of which was determined by the linear stability analysis of the corresponding two-dimensional flow. The recently developed IB solver [38] was used for conducting the three-dimensional simulations. Details of the implementation of the solver, along with its extensive verification for thermal flows in the presence of thermally active and passive immersed bodies, can be found in Ref. [38] and are omitted here for the sake of concision.

2.3. Verification study of the linear stability analysis

The verification study focuses on the analysis of the natural convection flow around two cylinders confined in a square cavity (see Fig. 2). The ratio between the cylinder diameter, d, and the cavity side length, L, is equal to $d/L=0.2$. The cylinders are aligned along the cavity's vertical centerline and are symmetrically distanced from the cavity's horizontal centerline. The distance δ between the cylinder centers, normalized by the cavity side of length L, is equal to $\delta=0.5$. Both cylinders are held at a constant hot temperature $\theta_H=1$, whereas all the cavity boundaries are held at a constant cold temperature, $\theta_C=0$. The force of gravity acts in the $-\hat{y}$ direction. The above configuration was chosen for two main reasons. First, it is relevant to the configurations under consideration in the present study, the only exception being that the porous media are modelled by thermally passive unconnected thin-walled cylinders, characterized by zero temperature gradient in the radial direction. Second, the considered flow undergoes a transition to unsteadiness through the first Hopf bifurcation [39], which allows us to compare the patterns of the absolute values of the leading eigenvectors of the temperature and velocity fields obtained by the linear stability analysis with those obtained by calculation of the time averaged maximal oscillation amplitudes.[2]

Fig. 3 presents a comparison between the contours of the leading eigenvectors obtained for u_x, u_y and θ fields and the corresponding contours of the oscillating amplitudes averaged over 20 oscillating periods. Both simulations were performed on 500×500 grids. The excellent agreement between the corresponding spatial distributions verifies the correctness of the performed linear stability analysis. Note the significant quantitative discrepancy observed between the values of the oscillation amplitudes and the absolute values of the corresponding eigenvectors. This fact is not surprising, since the magnitude of the leading eigenvector obtained by the linear stability analysis indicates the spatial distribution of the intensity of the oscillations exhibited in bifurcated flow and is determined up to multiplication by a constant.

3. Results and discussion

In this section, the concept of "smart" thermally insulating materials is presented first for 2D confined natural convection flow. The square differentially heated cavity with perfectly thermally conducting horizontal boundaries is used as a test bed. Thereafter, the proposed concept is validated for the realistic 3D flow in a differentially heated cubic cavity with thermally perfectly conducting lateral walls and all no-slip boundaries.

3.1. "Smart" thermally insulating materials for 2D flows

The heat flux through the differentially heated cavity can be estimated by calculation of the average Nusselt number, Nu, at the cavity boundaries, which for the no-slip boundary conditions depends only on the temperature gradient normal to the wall direction. Note that the temperature distribution of the considered steady state flow is skew-symmetric relative to the cavity center (i.e., $\theta(x,y)=\theta_H-\theta(L-x,L-y)$), and therefore the net heat flux is determined only by the average Nu values calculated at the vertical boundaries. At steady state, both Nu values should be equal to provide conservation of the total heat flux. It is commonly known (see e.g., [49,50]) that for this type of steady natural convection flow $Nu{\sim}Ra^{0.25}$. As the Rayleigh number increases, the flow undergoes a steady-unsteady transition through the first Hopf bifurcation. A further increase in the Ra number eventually leads to a turbulent flow regime, characterized by an increased heat flux through the cavity boundaries, governed by the $Nu{\sim}Ra^{0.33}$ relation [49,50].

It is clear that the most intuitive way to considerably decrease the heat flux through the cavity boundaries would be complete filling of the cavity interior with any kind of homogeneous thermal insulator. However, this naive approach would significantly increase the cost and the overall weight of such thermal insulation. Another alternative, embodying the key idea of the present study, is to considerably decrease the heat flux through the cavity boundaries by intelligently suppressing the momentum of the flow in accordance with a priori defined criteria. In the present study, we demonstrate the impact of local suppression of the momentum of the flow by positioning cylindrical thermally passive thin-walled obstacles of uniform diameter $d=0.04$ in the regions with maximal values of the criteria **A** and **B** defined in the previous section.

Fig. 4 demonstrates the procedure used for the design of a "smart" thermal insulator aimed at decreasing the heat flux for the natural convection flow inside a differentially heated cavity with thermally perfectly conducting lateral walls. The procedure is iterative and utilizes the **A** criterion. In the first iteration, the linear stability analysis is performed for the flow within the cavity without obstacles, yielding the value of the critical Rayleigh number, Ra_{cr}^0, for the first Hopf bifurcation. The corresponding fields of the values of **A** and the temperature distribution at steady state with the superimposed streamlines are shown in Fig. 4a. Thereafter, a pair of cylindrical obstacles are positioned at places

[2] The contours of the maximal time averaged amplitudes of bifurcated flow conveniently approximate the contours of the absolute values of the corresponding leading eigenvectors [46–48].

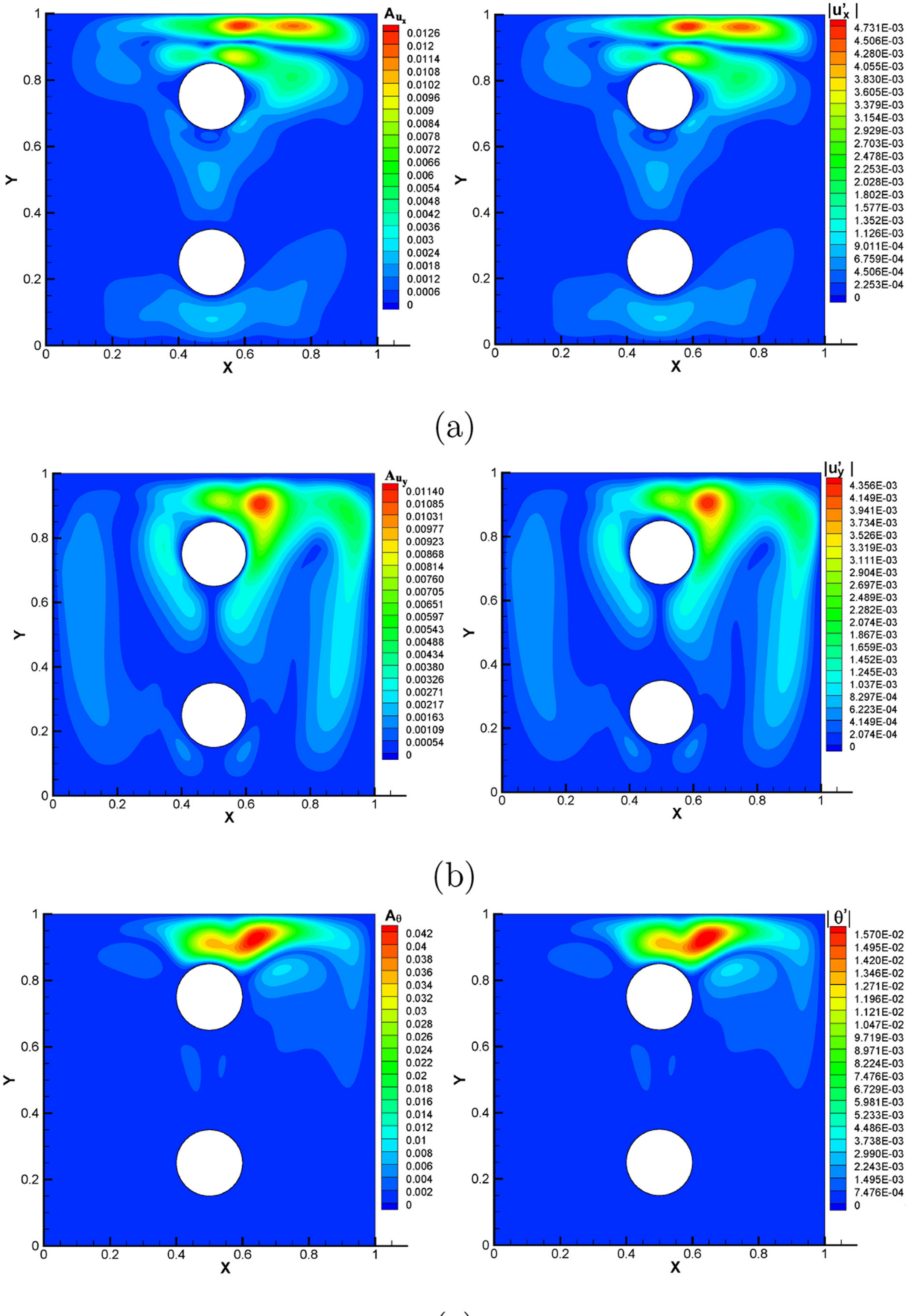

Fig. 3. Contours of the maximal amplitudes averaged over 20 oscillating periods and the corresponding absolute values of the leading eigenvectors obtained for: (a) velocity component u_x; (b) velocity component u_y; (c) temperature, θ. Both simulations were performed on 500×500 grids, $Ra = 5.0514 \times 10^5$.

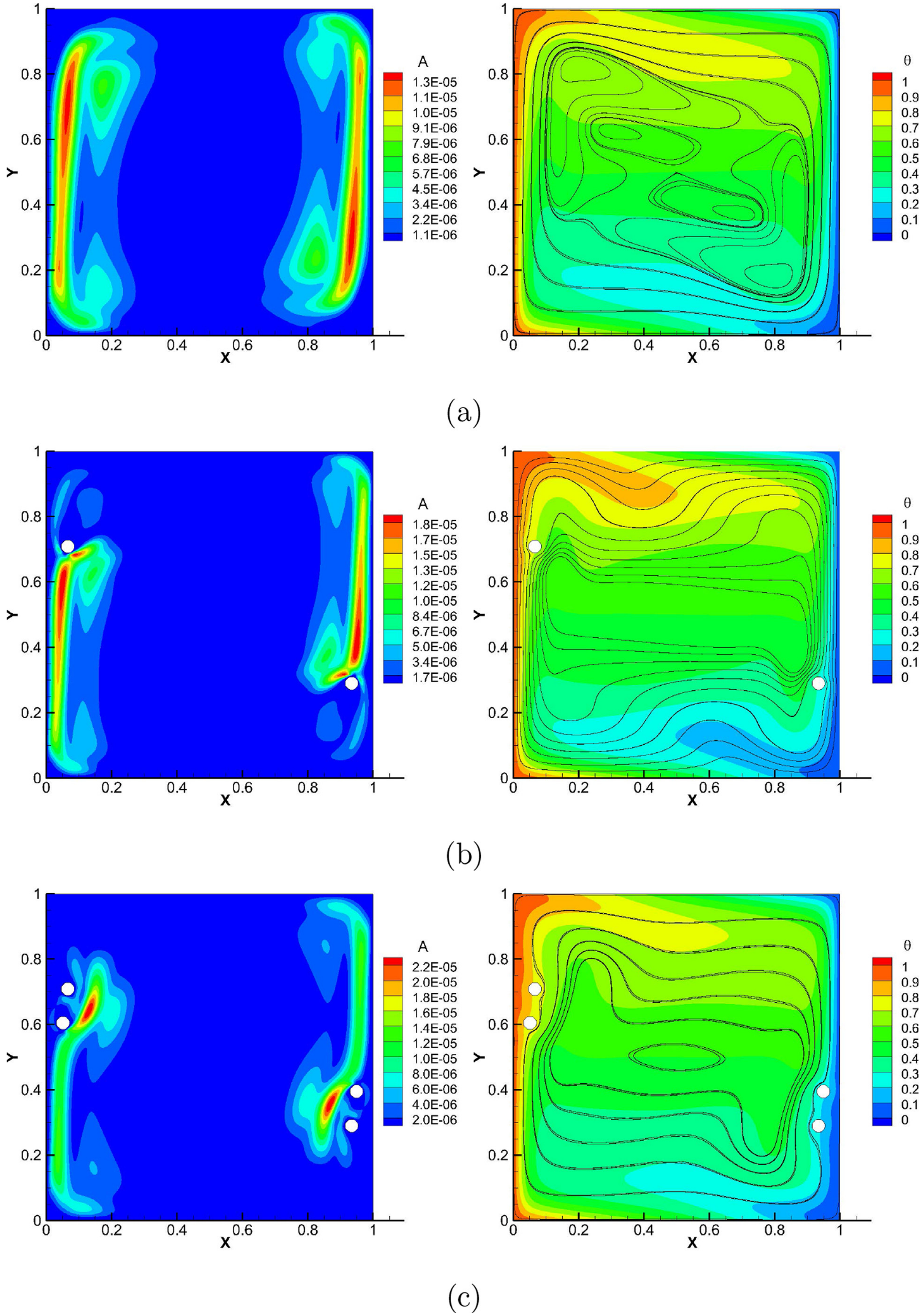

Fig. 4. Contours of criterion **A** and the corresponding steady state distribution of the temperature, θ with superimposed streamlines obtained at $Ra^0_{cr} = 2.11 \times 10^6$ for: (a) no obstacles; (b) 2 obstacles; (c) 4 obstacles; (d) 6 obstacles; (e) 8 obstacles; (f) 10 obstacles; (g) 20 obstacles; and (h) 40 obstacles. The diameter of all the obstacles is equal to d=0.04.

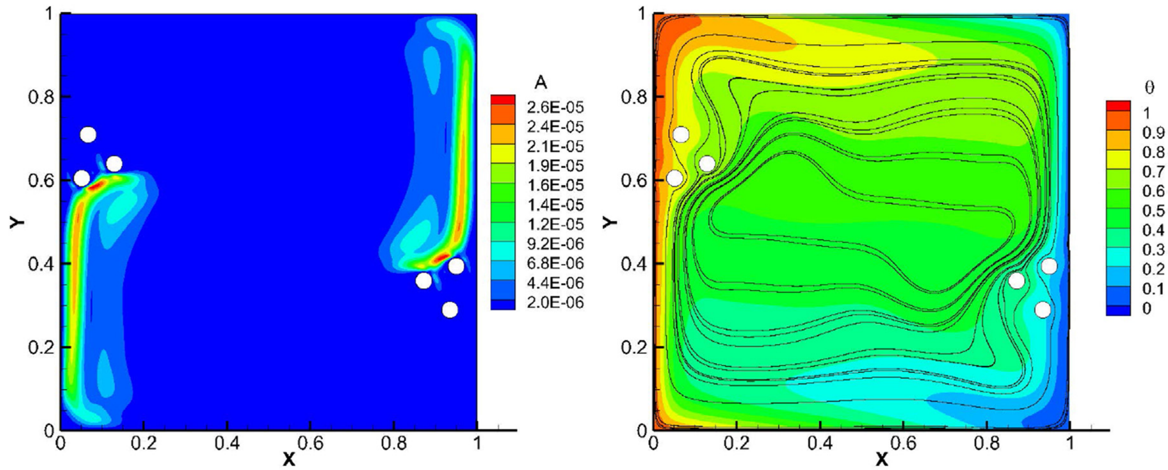

(d)

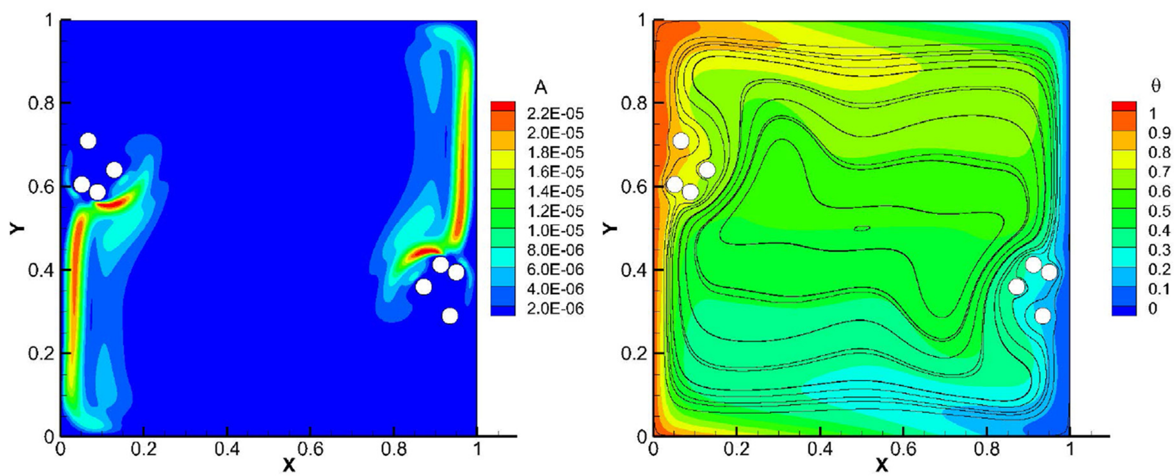

(e)

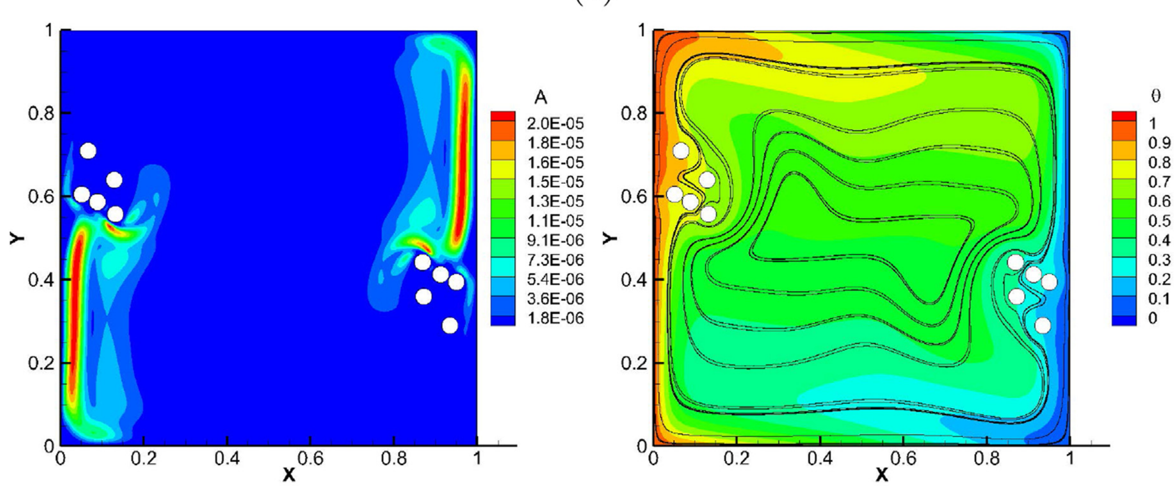

(f)

Fig. 4. (*continued*).

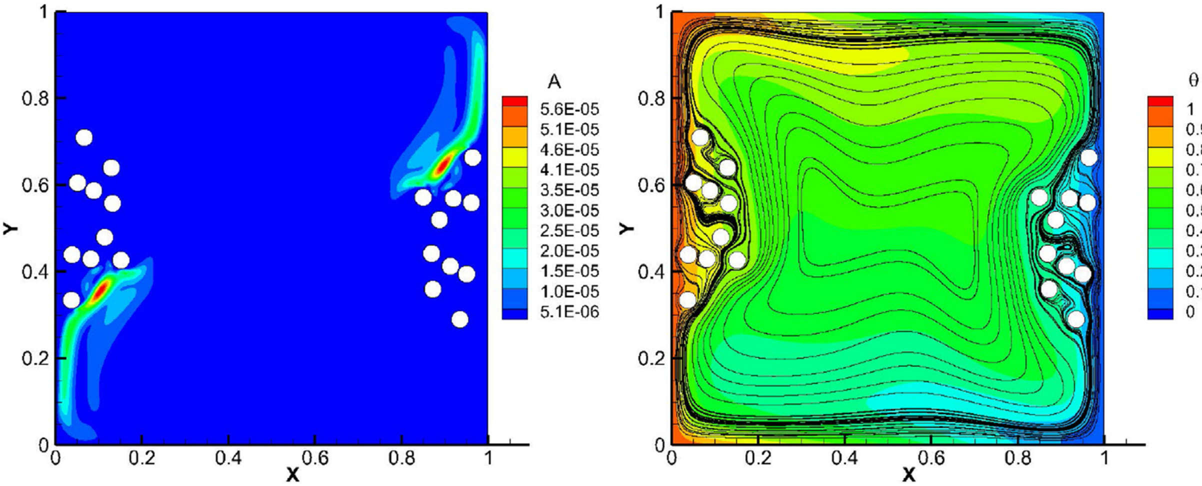

(g)

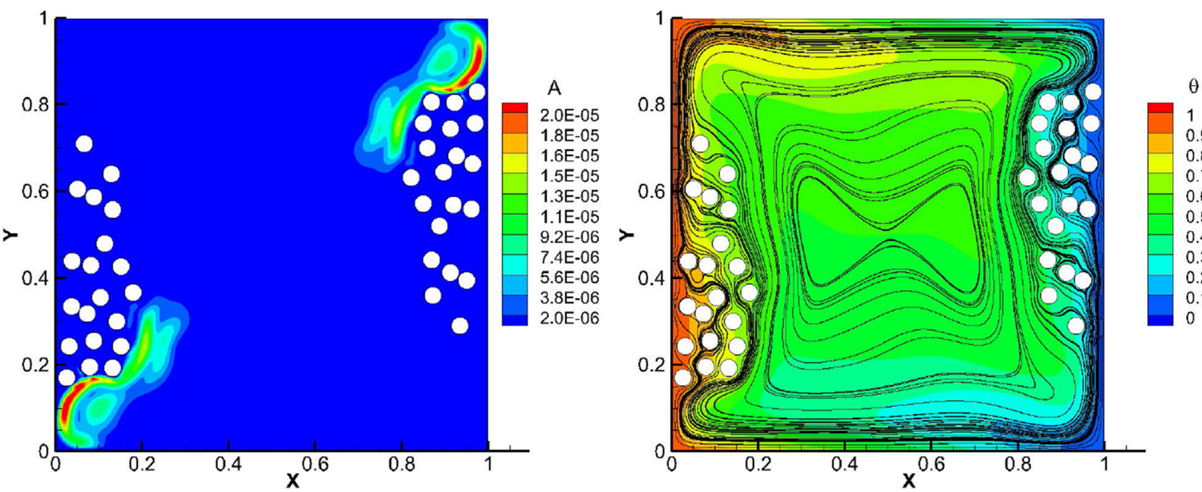

(h)

Fig. 4. (*continued*).

where **A** reaches its absolute maximum.[3] In the next step, the linear stability analysis is performed for the modified flow inside the cavity containing 2 embedded obstacles (see Fig. 4b). We then obtain a new value of Ra^2_{cr}, at which the modified flow characterized by a new distribution of **A** undergoes a transition to unsteadiness. Next, a pair of obstacles can again be positioned at places where the new values of **A** reach their absolute maximum. The above procedure is repeated until an a priori chosen stop condition − a twofold decrease in the average Nu number $Ra = Ra^0_{cr}$− is achieved. Fig. 4 (c−h) demonstrate the evolutionary stages of the modelled implants of porous media, which can be seen as a prototype for a “smart” thermally insulating material based on criterion **A**.

In the next stage, an alternative design for implanting the porous media was obtained by applying an iterative procedure based on the value of the second optimization parameter, **B**. The evolutionary stages of the design, corresponding to different numbers of embedded cylindrical obstacles, are shown in Fig. 5[4].

It should be stressed that in the present study the morphological structure of the modelled implants of porous media is restricted to unconnected packed beds (due to the limitations of the IB method). The above limitation can, however, be violated if the distance between any global maxima of **A** or **B** is equal or less than the diameter of the cylindrical obstacle. In addition none of the obstacles should touch or intersect any of the cavity boundaries. In both cases, the location of the next largest value of **A** or **B** is sought, and the morphological structure of the current ”candidate” for the porous media implant is tested for meeting all the restrictions. The procedure of seeking a new location for the next pair of cylindrical obstacles should be repeated until all the above restrictions are

[3] Note that for the configuration discussed, the distribution of **A** is skew-symmetric relative to the cavity center, i.e., $\mathbf{A}(x,y)=\mathbf{A}(L-x,L-y)$, and therefore the obstacles always come in pairs.

[4] Note that for the configuration discussed, the distribution of **B** is skew-symmetric relative to the cavity center, i.e., $\mathbf{B}(x,y)=\mathbf{B}(L-x,L-y)$, and therefore the obstacles always come in pairs.

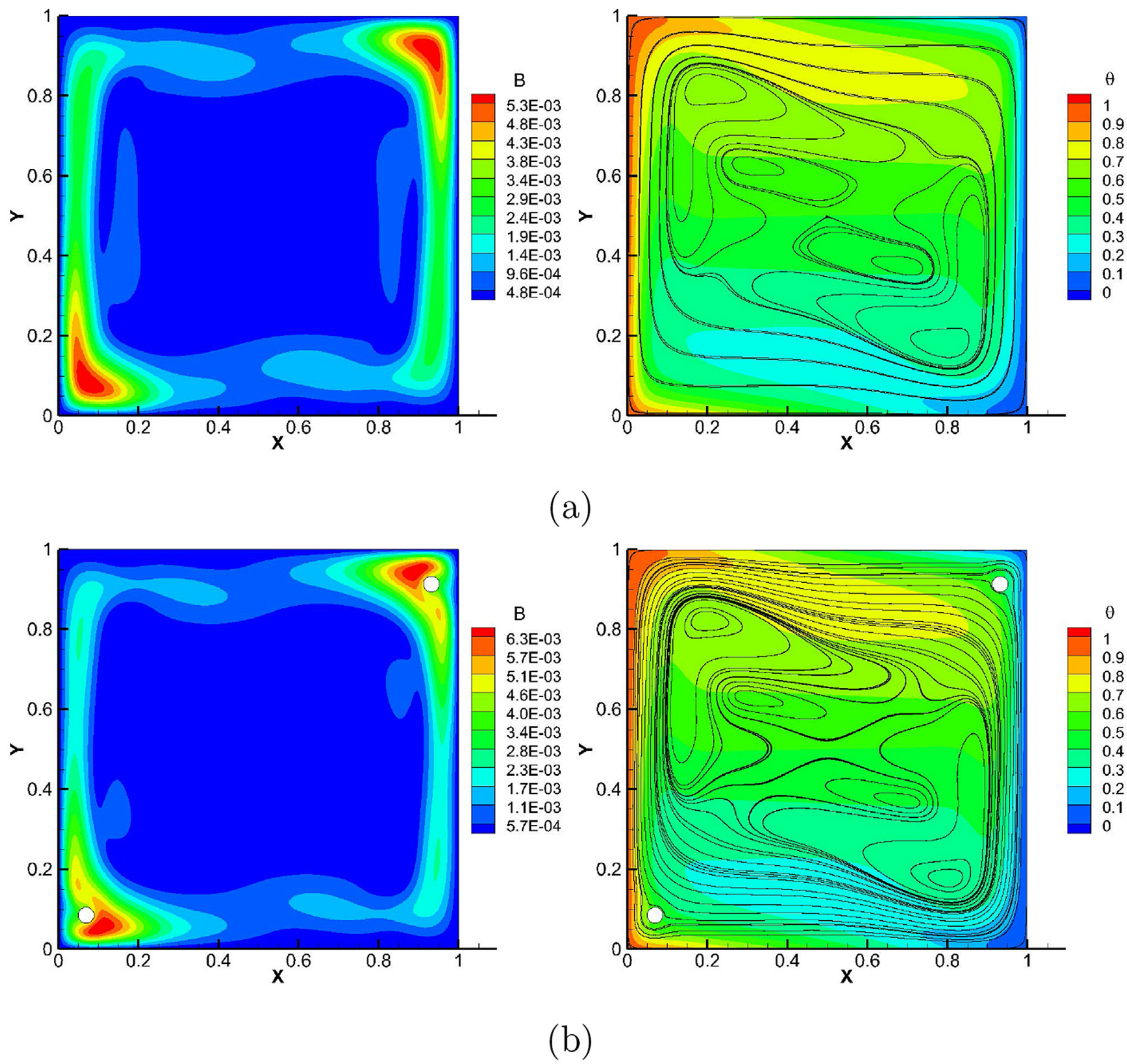

Fig. 5. Contours of criterion **B** and the corresponding steady state distribution of the temperature, θ with superimposed streamlines obtained at $Ra^0_{cr} = 2.11 \times 10^6$ for: (a) no obstacles; (b) 2 obstacles; (c) 4 obstacles; (d) 6 obstacles; (e) 8 obstacles; (f) 10 obstacles; (g) 20 obstacles; (h) and 40 obstacles. The diameter of all the obstacles is equal to d=0.04.

satisfied.[5]

Embedding cylindrical obstacles is characterised by a twofold mechanism, which can increase the insulating efficiency of the cavity. First, for the given value of the *Ra* number, it suppresses the overall momentum of the convective flow, which in turn leads to increasing thickness of thermal boundary layer and results in lower temperature gradients in the direction normal to the vertical walls. Second, it delays the onset of unsteadiness, which means that the natural convection flow in the cavity with embedded obstacles remains laminar and steady, even at rapidly increasing *Ra* numbers. The effect of both mechanisms was quantified as shown in Fig. 6.

Indistinguishable differences were observed for both average *Nu* and critical Ra_{cr} values obtained on 500×500 and 600×600 grids, which successfully verifies the grid independence of the results. It can be also seen that utilizing the implants of porous media designed in accordance with the first criterion **A** (see Fig. 6-a) allows for a rapid decrease of the average *Nu* number value, which attains half of its original value for 40 embedded cylinders[6] Note also that 40 cylinders occupy only 5% of the total volume of the cavity. The dependency of the Ra_{cr} value on the number of obstacles is not monotonic, although the Ra_{cr} of the final configuration consisting of 40 cylinders is higher by an order of magnitude than its original value.

The implants of porous media designed by utilizing the second criterion **B** (see Fig. 6b) exhibit much lower efficiency in terms of thermal insulation. In fact, embedding implants consisting of 40 cylinders (the same number as for criterion **A**) leads to only an approximately 20% decrease in the average *Nu* value. Moreover, after embedding 24 cylinders, the average *Nu* number reaches its asymptotic value, which does not deviate significantly with increasing numbers of embedded cylinders. Similarly to the

[5] Typically, only one iteration was required for the configurations considered in the present study.

[6] All the simulations were performed at Ra^0_{cr}=2.11×10^6, at which the flow without obstacles undergoes a steady-unsteady transition.

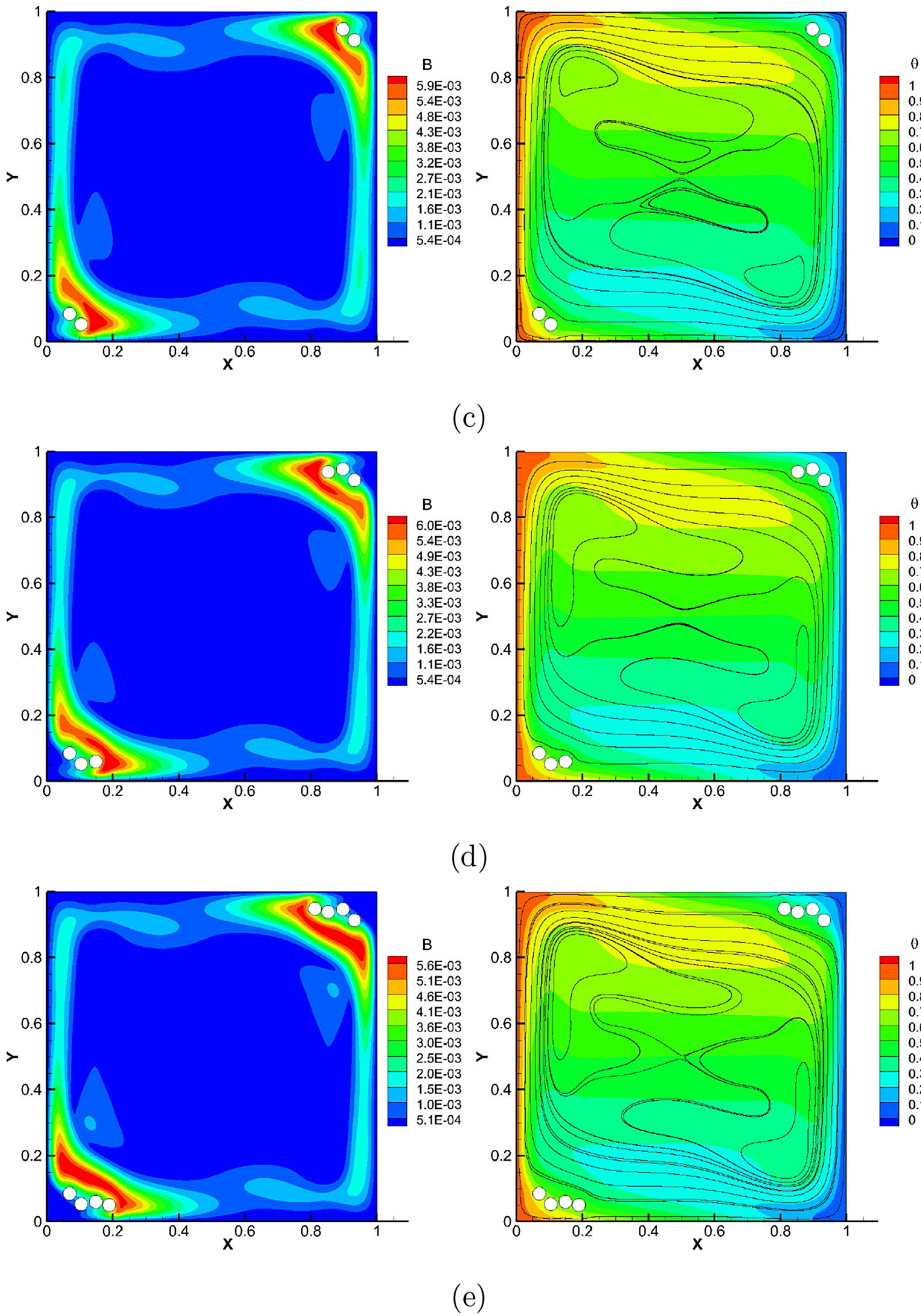

Fig. 5. (*continued*).

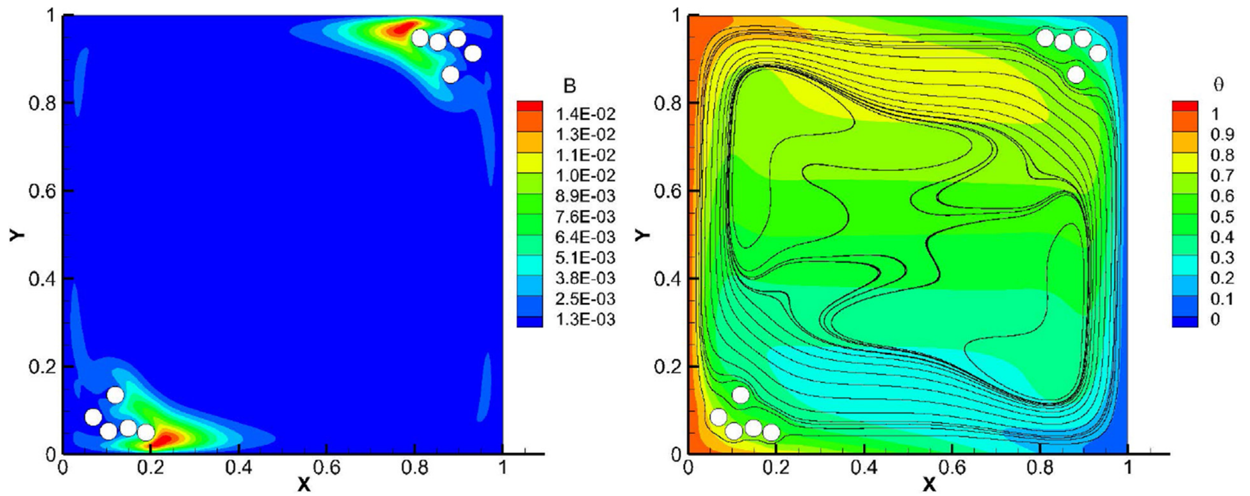

(f)

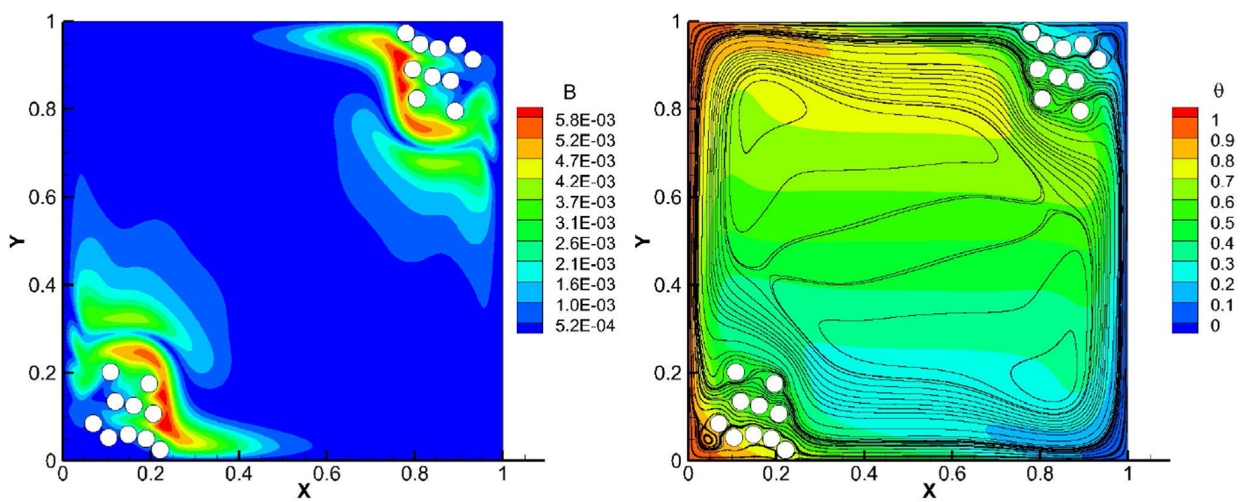

(g)

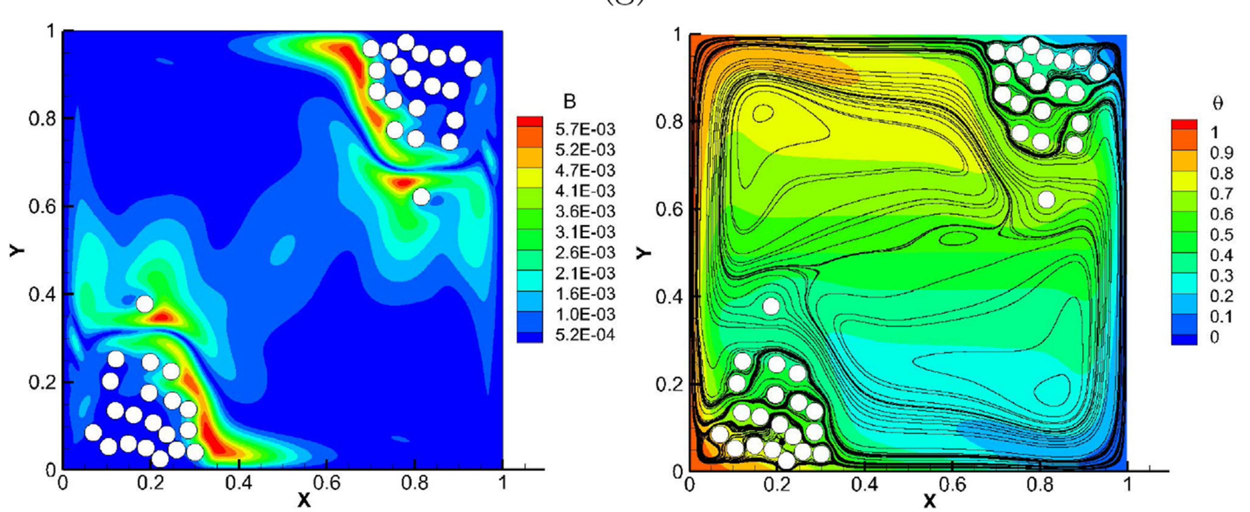

(h)

Fig. 5. (*continued*).

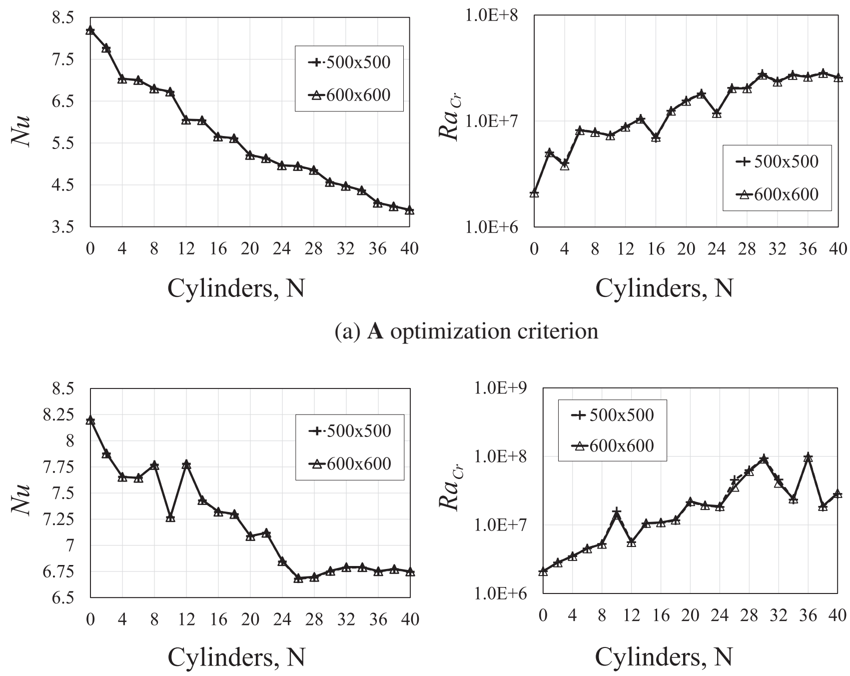

(a) **A** optimization criterion

(b) **B** optimization criterion

Fig. 6. Variation of the values of the averaged *Nu* number obtained for the vertical hot wall of the cavity at Ra_{cr}^0=2.11×10^6 and the critical Rayleigh number, Ra_{cr} for the steady-unsteady transition obtained by the linear stability analysis as a function of the number of cylindrical obstacles for: (a) **A** optimization criterion; (b) **B** optimization criterion. The calculations were performed on 500×500 and 600×600 grids.

previous configuration, the dependency of the Ra_{cr} value on the number of obstacles is not monotonic. It is remarkable that here too a difference of one order of magnitude is observed between the initial and final values of Ra_{cr}. It is worth noting that a similar trend was also observed by Costa et al., who reported a 30% decrease in the average *Nu* value [51] when investigating the influence of solid inserts placed at the inner corners of differentially heated square enclosures, where the thermal conductivity of the inserts was equal to or less than that of the fluid. According to the authors, the rationale for the choice of those inserts could be explained by the stagnation regions that develop in the vicinity of the corners. In the present study, we revisit and explain formally the observed decrease of the heat flux by means of a linear stability analysis of the natural convection flow.

3.2. "Smart" thermally insulating materials for 3D flows

In this section the concept of "smart" thermally insulating materials is validated for realistic 3D flows. The 2D configurations containing implants of porous media embedded into the square differentially heated cavity are extended in the direction normal to the plane of the 2D cavity. As a result, the original 2D configurations are transformed into their 3D analogs, comprising cubic differentially heated cavities with thermally perfectly conducting lateral walls and all no-slip boundaries. The 2D circular obstacles are, in turn, transformed into 3D circular cylinders, extending over the entire width of the cavity. An example of four such 3D configurations, corresponding to the optimization criteria **A** and **B** with patterns containing 20 and 40 cylinders, are shown in Fig. 7.

All the simulations were performed for Ra=2.11×10^6 corresponding to the value of the critical Rayleigh number Ra_{cr}^0 that characterizes the transition to unsteadiness of the 2D flow inside a differentially heated cavity with thermally perfectly conducting horizontal walls. We note in passing that for a differentially heated cavity Ra_{cr2D}<Ra_{cr3D} due to the damping effect of the lateral walls, which determines the steady state regime of all the 3D flows considered in the present study. It is assumed that convergence to steadiness is reached when the maximal point-wise relative difference for the field at two consecutive time steps is less than 10^{-5}. Note also the striking resemblance between the 3D and the corresponding 2D temperature distributions (see Fig. 4-g,h and Fig. 5-g,h), which is typical of this kind of convective flow.

Table 1 presents the grid independence study for the *Nu* values averaged over the hot wall of the cavity as a function of the number of embedded obstacles. The results were obtained on 200^3, 300^3 and 400^3 grids. It can be seen that the maximum deviation in the averaged *Nu* values for 300^3 and 400^3 grids did not exceed 1%, thereby successfully verifying the grid independence of the results. All the calculations of the 3D flow presented further in this section were obtained on a 400^3 computational grid. It was also verified (not shown here) that the values of *Nu* numbers averaged over the hot and the cold walls were equal up to the fourth decimal digit, which proves conservation of the overall heat flux through the cavity boundaries.

The final validation of the concept of "smart" thermally insulating materials designed by utilizing both **A** and **B** optimization criteria for 2D and 3D flows is summarized in Table 2. It is remarkable that in the 3D differentially heated cavity, the ultimate morphology of the implants of porous media designed by utilizing both **A** and **B** criteria and consisting of 40 cylinders consistently yielded about the same decrease in the average *Nu* value (i.e. about a two fold decrease for the criterion **A** and about 20% for the criterion **B**) as that observed for the corresponding 2D configuration.

4. Summary and conclusions

The concept of the design of "smart" thermally insulating

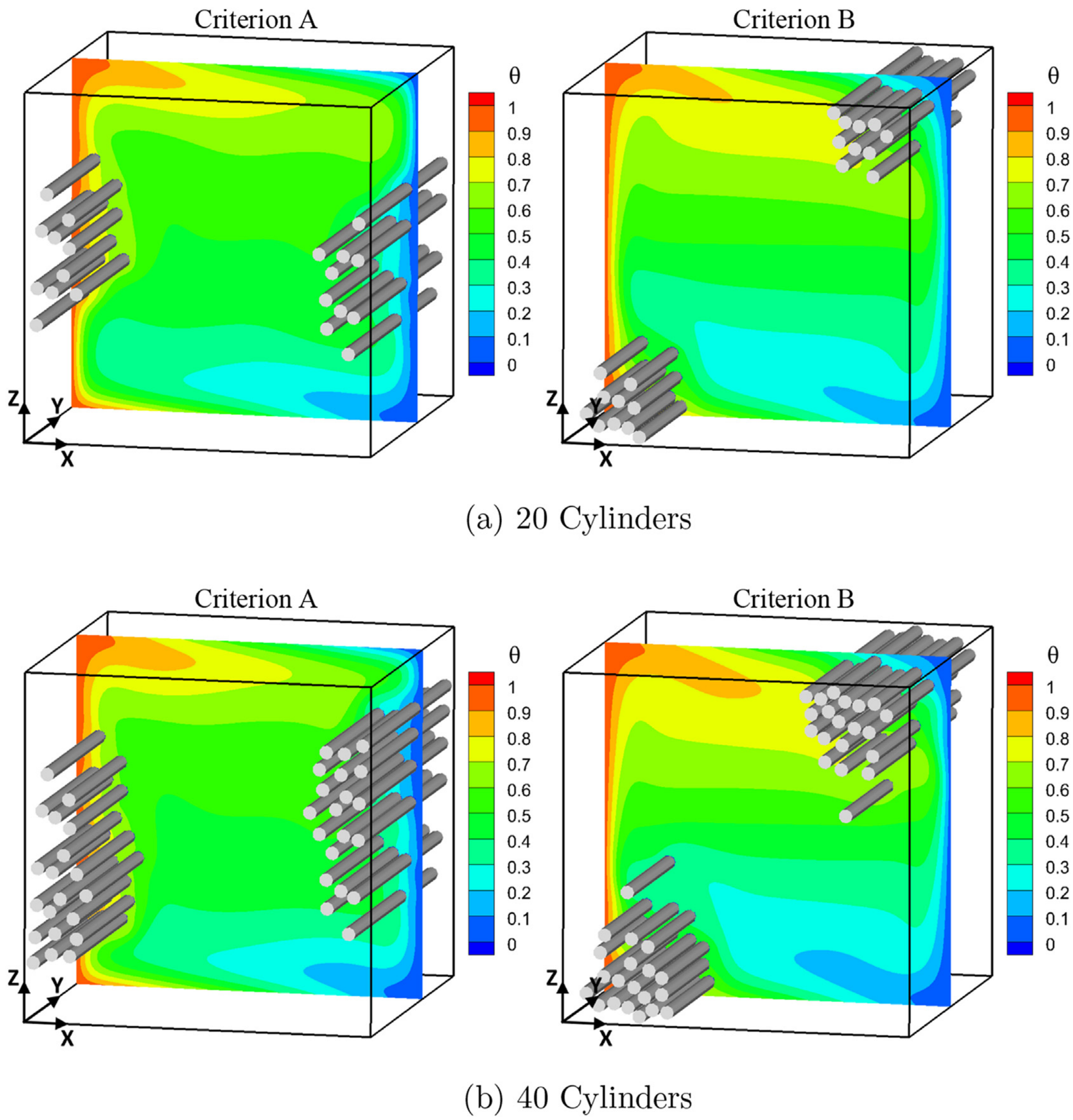

Fig. 7. 3D setup obtained by extension of the corresponding 2D configurations in the *z* direction with a superimposed temperature distribution at the mid cross-section of the cavity obtained at $Ra=2.11\times10^6$ by: (a) 20 cylinders, the location of which was obtained by utilizing optimization criteria **A** and **B**; and (b) 40 cylinders, the location of which was obtained by utilizing optimization criteria **A** and **B**.

Table 1
Verification of the grid independence of the averaged *Nu* values calculated at the hot wall of the cubic cavity for $Ra=2.11\times10^6$. Values in the Table are averaged *Nu* values.

Number of cylinders, N	Criterion A for grid			Criterion B for grid		
	200^3	300^3	400^3	200^3	300^3	400^3
0	8.353	8.353	8.353	8.353	8.353	8.353
10	6.449	6.506	6.552	7.043	6.985	6.992
20	4.943	5.087	5.126	6.588	6.755	6.724
30	4.281	4.327	4.356	6.333	6.426	6.328
40	3.535	3.569	3.589	6.214	6.340	6.328

Table 2
Validation of the concept of "smart" thermally insulating materials for 2D and 3D flows. The *Nu* values presented in the Table were averaged over hot wall of the differentially heated cavity with all thermally perfectly conducting horizontal (2D) and lateral (3D) walls.

Number of cylinders, *N*		0	10	20	30	40
Criterion **A**	2D	8.200	6.728	5.215	4.568	3.906
Criterion **B**		8.200	7.270	7.089	6.756	6.750
Criterion **A**	3D	8.353	6.552	5.126	4.356	3.589
Criterion **B**		8.353	6.992	6.724	6.328	6.328

materials based on heterogeneous thermally passive porous media was established and extensively validated for both 2D and 3D confined natural convection flows. The porous medium was modelled by unconnected packed beds of circular cylinders. The location of each cylinder was determined by an iterative procedure based on a linear stability analysis of the flow fields. The effect of optimization criteria **A** and **B**, related to perturbation of the velocity and temperature fields, respectively, on the insulation properties of 2D and 3D differentially heated cavities was extensively investigated. It was found that for the given value of *Ra* the implants of porous media designed by utilizing criterion **A** and occupying only 5% of the total volume can decrease the overall heat flux by a factor of 2 through the boundaries of both 2D and 3D differentially heated cavities. In contrast, the implants of porous media designed by using criterion **B** decreased the heat flux by only 20% for both 2*D* and 3*D* configurations. Implants of porous media designed by both criteria delayed the transition to unsteadiness of the 2*D* natural convection flow, which was reflected by an increase in the critical Ra_{cr} value by an order of magnitude when using the ultimate patterns (consisting of 40 cylinders) of implants of both types.

The present work thus summarizes our first effort aimed at developing a formal systematic methodology for establishing a concept for the design of "smart" thermally insulating materials. Although the concept of smart thermal insulation was demonstrated here only for differentially heated cavities, the established methodology is general and is not restricted to this particular geometry. In practice, smart insulation materials, built of heterogeneous porous media, can be intelligently adapted to any specified engineering configuration, including both natural and forced convection regimes. For the forced convection regime the pressure drop imposed by the modelled porous media should be accounted when estimating the overall insulating efficiency of the system. In the present study, the heterogeneous porous medium was modelled by unconnected packed beds of equi-sized circular cylinders (both 2D and 3D), which is a particular case of realistic porous media typically built of pores of varying sizes. Generalization of the results obtained in the present study for heterogeneous porous media modelled by cylinders of varying sizes requires statistical evaluation of a whole set of "similar" systems and will be the focus of our future studies.

References

[1] Baytas A, Pop I. Free convection in oblique enclosures filled with a porous medium. Int J Heat Mass Transf 1999;42:1047–57.
[2] Tang DL, Li LP, Song CF, Tao WQ, He YL. Numerical theramal analysis of applying insulation material to holes in hollow brick walls by the finite-volume method. Numer Heat Transf Part A 2015;68:526–47.
[3] Bhattacharyya S, Singh AK. Augmentation of heat transfer from a solid cylinder wrapped with a porous layer. Int J Heat Mass Transf 2009;64:1991–2001.
[4] Bruneau CH, Mortazavi I. Numerical modelling and passive flow control using porous media. Comput Fluid 2008;46:488–98.
[5] Nassehi V. Modeling of combined navier-stokes and darcy flows in crossflow membrane filtration. Comput Fluid 1998;53:1253–65.
[6] Joslin RD. Aircraft laminar flow control. Comput Fluid 1998;30:1–29.
[7] Majdalani J, Zhou C, Dawson CA. Two-dimensional viscous flow between slowly expanding or contracting walls with weak permeability. J Biomech 2002;35:1399–403.
[8] Berkowitz B. Characterizing flow and transport in fractured geological media: a review. Water Resour 2002;25:861–84.
[9] Vafai K, Tien CL. Boundary and inertia effects on flow and heat transfer in porous media. Int J Heat Mass Transf 1981;26:195–203.
[10] Antohe BV, Lage JL. A general two-equation macroscopic turbulence model for incompressible flow in porous media using unit cell scale. Int J Heat Mass Transf 1997;40:3013–24.
[11] Silva RA, de Lemos MJS. Turbulent flow in channel occupied by a porous layer considering the stress jump at the interface. Int J Heat Mass Transf 2003;26:5113–21.
[12] Antohe BV, Lage JL. The laminar boundary layer over a permeable wall. Transp Porous Media 2005;59:267–300.
[13] Pereira JCF, Malico I, Hayashi TC, Raposo JMF. Experimental and numerical characterization of the transverse dispersion at the exit of a short ceramic foam inside a pipe. Int J Heat Mass Transf 2005;40:3013–24.
[14] Pereira JCF, Malico I, Hayashi TC, Raposo JMF. Study of high reynolds number pipe flows with porous inserts. Int J Heat Mass Transf 2012;15:549–63.
[15] Qiu H, Lage JL, Junqueira SLM, Franco AT. Predicting the Nusselt number of heterogeneous (porous) enclosures using a generic form of the Berkovsky-Polevikov correlations. J Heat Transf 2013;135:082601.
[16] Martin AR, Saltiel C, Shyy W. Frictional losses and convective heat transfer in sparse, periodic cylinder arrays in cross flow. Int J Heat Mass Transf 1998;41:2382–97.
[17] Keyser MJ, Conradie M, Coertzen M, Van Dyk JC. Effect of coal particle size distribution on packed bed pressure drop and gas flow distributions. Fuel 2006;85:1439–45.
[18] Narvaez A, Yazdchi K, Luding S, Harting J. From creeping to inertial flow in porous media: a lattice boltzmann finite element study. J Stat Mech 2013:P02038.
[19] Jafari A, Zamankhana P, Mousavi S, Pietarnien K. Modeling and CFD simulation of flow behavior and dispersivity through randomly packed reactors. Chem Eng J 2008:476–82.
[20] Van der Hoef MA, Beetstra R, Kuipers JAM. Lattice-Boltzmann simulations of low Reynolds-number flow past mono- and bidisperse arrays of spheres: results for the permeability and drag force. J Fluid Mech 2005;528:233–54.
[21] Beetstra R, Van der Hoef MA, Kuipers JAM. Drag force of intermediate Reynolds number flow past mono- and bidisperse arrays of sphere. AIChE J 2007;53:489–501.
[22] Yin X, Sundaresan S. Drag force of intermediate Reynolds number flow past mono- and bidisperse arrays of sphere. Ind Eng Chem Res 2009;48:227–41.
[23] Sangani AS, Yao C. Transport process in random arrays of cylinders. II. Viscous flow. Phys Fluids 1988;31:2435–44.
[24] Clague DS, Phillips RJ. A numerical calculation of the hydraulic permeability of three-dimensional disordered fibrous media. Phys Fluids 1997;9:1562–72.
[25] Maier RS, Kroll DM, Davis HT, Bernard RS. Simulation of flow in bidisperse sphere packings. J Colloid Interface Sci 1999;217:341–7.
[26] Garcia X, Akanji LT, Blunt MJ, Matthai SK, Latham JP. Numerical study of the effects of particle shape and polydispersivity on permeability. Phys Rev E 2009;80:021304.
[27] Liu HL, Hwang WR. Permeability prediction of fibrous porous media with complex 3d architectures. Compos Part A 2012;43:2030–8.
[28] Al-Hazmi MM. Analysis of coupled natural convectionconduction effects on the heat transport through hollow building blocks. Energy Build 2006;38:515–21.
[29] Al-Hazmi MM. Numerical investigation on using inclined partitions to reduce natural convection inside the cavities of hollow bricks. Int J Therm Sci. 2010;49:2201–10.
[30] Laguerre O, Benamara S, Remy D, Flick D. Experimental and numerical study of heat and moisture transfers by natural convection in a cavity filled with solid obstacles. Int J Heat Mass Transf 2009;52:5691–700.
[31] Banerjee S, Mukhopadhyay A, Sen S, Ganguly G. Natural convection in a bi-heater configuration of passive electronic cooling. Int J Therm Sci. 2008;47:1516–27.
[32] Nardini G, Paroncini M. Heat transfer experiment on natural convection in a square cavity with discrete sources. Heat Mass Transf 2012;48:1855–65.
[33] Peskin CS. Flow patterns around heart valves: a numerical method. J Comput Phys 1972;10:252–71.
[34] Roma A, Peskin CS, Berger MJ. An adaptive version of the immersed boundary method. J Comput Phys 1999;153:509–34.
[35] Uhlmann M. An immersed boundary method with direct forcing for the simulation of particulate flows. J Comput Phys 2005;209:448–76.
[36] Taira K, Colonius T. The immersed boundary method: a projection approach. J Comput Phys 2007;225:3121–33.
[37] Kempe T, Fröhlich J. An improved immersed boundary method with direct forcing for the simulation of particle laden flows. J Comput Phys 2012;231:3663–84.
[38] Gulberg Y, Feldman Y. On laminar natural convection inside multi-layered spherical shells. Int J Heat Mass Transf 2015;91:908–21.
[39] Feldman Y, Gulberg Y. An extension of the immersed boundary method based on the distributed Lagrange multiplier approach. J Comput Phys 2016;322:248–66.
[40] Beyer RP, LeVeque RJ. Analysis of a one-dimensional model for the immersed boundary method. SIAM J Numer Anal 1992;29:332–64.
[41] Giannetti F, Luchini P. Structural sensitivity of the first instability of the cylinder wake. J Fluid Mech 2007;581:167–97.
[42] Kallemov B, Bhalla A, Griffith BE, Donev A. An immersed boundary method for rigid bodies. 2015. arXiv:1505.07865.
[43] Mohd-Yusof J. Combined immersed-boundary/b-spline methods for simulations of flow in complex geometries. Center for turbulence research, annual research briefs. 1997. p. 317–27.
[44] Faldun A, Verzicco E,R, Orlandi P, Mohd-Yusof J. Combined immersed-boundary finite-difference methods for three-dimensional complex flow simulations. J Comput Phys 2000;161:35–60.
[45] Gelfgat A. Oscillatory instability of three-dimensional natural convection of air in a laterally heated cubic box. 2015. arXiv:1508.00652.
[46] Theofilis V, Duck PW, Owen J. Viscous linear stability analysis of rectangular duct and cavity flow. J Fluid Mech 2005;505:249–86.
[47] Feldman Y, Gelfgat AY. Oscillatory instability of a three-dimensional lid-driven flow in a cube. Phys Fluids 2010;22:093602.
[48] Feldman Y. Theoretical analysis of three-dimensional bifurcated flow inside a diagonally lid-driven cavity. Theor Comput Fluid Dynam 2015;29:245–61.
[49] Xamán J, Álvarez G, Lira L, Estrada C. Numerical study of heat transfer by laminar and turbulent natural convection in tall cavities of façade elements. Energy Build 2005;37:787–94.
[50] Yin K, Wung T, C. K. Natural convection in air layer enclosed within rectangular cavities. Int J Heat Mass Transf 1978;21:307–15.
[51] Costa VAF, Oliveira MSA, S. A. C. M. Control of laminar natural convection in differentially heated square enclosures using solid inserts at the corners. Int J Heat Mass Transf 2003;46:3529–37.